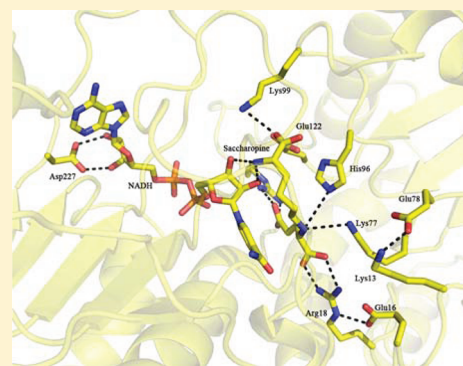


# Evidence in Support of Lysine 77 and Histidine 96 as Acid–Base Catalytic Residues in Saccharopine Dehydrogenase from *Saccharomyces cerevisiae*

Vidya Prasanna Kumar, Leonard M. Thomas, Kostyantyn D. Bobyk, Babak Andi, Paul F. Cook,\* and Ann H. West\*

Department of Chemistry and Biochemistry, University of Oklahoma, 101 Stephenson Parkway, Norman, Oklahoma 73019, United States

**ABSTRACT:** Saccharopine dehydrogenase (SDH) catalyzes the final reaction in the  $\alpha$ -aminoadipate pathway, the conversion of L-saccharopine to L-lysine (Lys) and  $\alpha$ -ketoglutarate ( $\alpha$ -kg) using NAD<sup>+</sup> as an oxidant. The enzyme utilizes a general acid–base mechanism to conduct its reaction with a base proposed to accept a proton from the secondary amine of saccharopine in the oxidation step and a group proposed to activate water to hydrolyze the resulting imine. Crystal structures of an open apo form and a closed form of the enzyme with saccharopine and NADH bound have been determined at 2.0 and 2.2 Å resolution, respectively. In the ternary complex, a significant movement of domain I relative to domain II that closes the active site cleft between the two domains and brings H96 and K77 into the proximity of the substrate binding site is observed. The hydride transfer distance is 3.6 Å, and the side chains of H96 and K77 are properly positioned to act as acid–base catalysts. Preparation of the K77M and H96Q single-mutant and K77M/H96Q double-mutant enzymes provides data consistent with their role as the general acid–base catalysts in the SDH reaction. The side chain of K77 initially accepts a proton from the  $\epsilon$ -amine of the substrate Lys and eventually donates it to the imino nitrogen as it is reduced to a secondary amine in the hydride transfer step, and H96 protonates the carbonyl oxygen as the carbinolamine is formed. The K77M, H976Q, and K77M/H96Q mutant enzymes give 145-, 28-, and 700-fold decreases in  $V/E_t$  and  $>10^3$ -fold increases in  $V_2/K_{Lys}E_t$  and  $V_2/K_{\alpha\text{-kg}}E_t$  (the double mutation gives  $>10^5$ -fold decreases in the second-order rate constants). In addition, the K77M mutant enzyme exhibits a primary deuterium kinetic isotope effect of 2.0 and an inverse solvent deuterium isotope effect of 0.77 on  $V_2/K_{Lys}$ . A value of 2.0 was also observed for  $^D(V_2/K_{Lys})_{D_2O}$  when the primary deuterium kinetic isotope effect was repeated in  $D_2O$ , consistent with a rate-limiting hydride transfer step. A viscosity effect of 0.8 was observed on  $V_2/K_{Lys}$ , indicating the solvent deuterium isotope effect resulted from stabilization of an enzyme form prior to hydride transfer. A small normal solvent isotope effect is observed on  $V$ , which decreases slightly when repeated with NADD, consistent with a contribution from product release to rate limitation. In addition,  $V_2/K_{Lys}E_t$  is pH-independent, which is consistent with the loss of an acid–base catalyst and perturbation of the  $pK_a$  of the second catalytic group to a higher pH, likely a result of a change in the overall charge of the active site. The primary deuterium kinetic isotope effect for H96Q, measured in  $H_2O$  or  $D_2O$ , is within error equal to 1. A solvent deuterium isotope effect of 2.4 is observed with NADH or NADD as the dinucleotide substrate. Data suggest rate-limiting imine formation, consistent with the proposed role of H96 in protonating the leaving hydroxyl as the imine is formed. The pH–rate profile for  $V_2/K_{Lys}E_t$  exhibits the  $pK_a$  for K77, perturbed to a value of  $\sim 9$ , which must be unprotonated to accept a proton from the  $\epsilon$ -amine of the substrate Lys so that it can act as a nucleophile. Overall, data are consistent with a role for K77 acting as the base that accepts a proton from the  $\epsilon$ -amine of the substrate lysine prior to nucleophilic attack on the  $\alpha$ -oxo group of  $\alpha$ -ketoglutarate, and finally donating a proton to the imine nitrogen as it is reduced to give saccharopine. In addition, data indicate a role for H96 acting as a general acid–base catalyst in the formation of the imine between the  $\epsilon$ -amine of lysine and the  $\alpha$ -oxo group of  $\alpha$ -ketoglutarate.



Saccharopine dehydrogenase [N6-(glutaryl-2)-L-lysine:NAD oxidoreductase, EC 1.5.1.7] (SDH) catalyzes the final step in the  $\alpha$ -aminoadipate (AAA) pathway for the de novo synthesis of L-lysine in fungi.<sup>3,4</sup> The enzyme catalyzes the reversible pyridine nucleotide-dependent oxidative deamination of saccharopine to generate  $\alpha$ -kg and Lys using NAD as an oxidant (Scheme 1).<sup>3</sup>

The proposed kinetic mechanism for the *Saccharomyces cerevisiae* SDH is ordered in the physiologic reaction direction

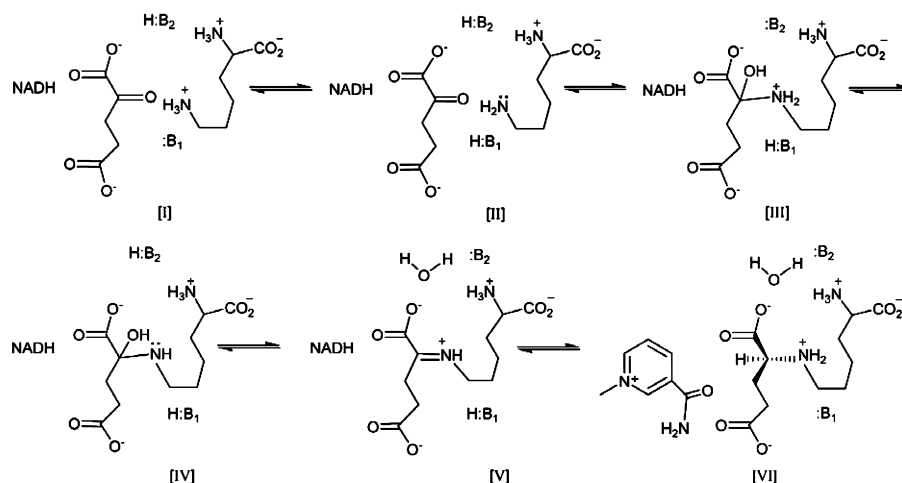
with NAD binding before saccharopine (Sacc), while in the opposite direction,  $\alpha$ -ketoglutarate ( $\alpha$ -kg) and lysine (Lys) bind in a random fashion once NADH is bound.<sup>5</sup> A chemical mechanism involving two acid–base catalytic groups has been

**Received:** December 8, 2011

**Revised:** January 11, 2012

**Published:** January 13, 2012



Scheme 1. Chemical Mechanism Proposed for Saccharopine Dehydrogenase<sup>a</sup>


<sup>a</sup>The reaction is written in the direction of Sacc formation: (I) protonated Lys, (II) formed central E-NADH- $\alpha$ -kg-Lys complex, (III) protonated carbinolamine, (IV) carbinolamine intermediate, (V) Schiff base intermediate, and (VI) hydride transfer and formation of Sacc. With the exception of Sacc, no stereochemistry is implied.

proposed on the basis of the pH dependence of kinetic parameters (Scheme 1).<sup>6</sup> Once the E-NADH- $\alpha$ -kg-Lys central complex is formed, the first base ( $B_1$ ) accepts a proton from the  $\epsilon$ -amine of Lys to allow nucleophilic attack on the carbonyl of  $\alpha$ -kg (II). Nucleophilic attack gives a protonated carbinolamine with donation of a proton from the conjugate acid of  $B_2$  to the carbonyl oxygen (III). The conjugate base of  $B_2$  then accepts a proton from the carbinolamine nitrogen (IV), and this is followed by elimination of water to give the imine (V), which is reduced by NADH concomitant with protonation of the imine nitrogen by the conjugate acid of  $B_1$ . A number of residues (E78, E122, K99, and D319) in the active site of SDH have been mutated, and mutant enzymes have been characterized.<sup>7,8</sup> To date, none appear to serve as acid–base catalytic residues.

In this study, the roles of K77 and H96 have been determined by mutating them to M and Q, respectively. Mutations of K77 and H96 were prepared in the C205S mutant enzyme, which eliminates disulfide formation, so that 100% of the enzyme is in the “reduced” active form.<sup>1</sup> A 1.6 Å X-ray structure the wild-type SDH apoenzyme was determined by the Berghuis group<sup>9</sup> and showed a tertiary fold consisting of two domains (I and II) with a narrow cleft between them. Each domain can be described as a modified nucleotide-binding Rossmann-like fold. The active site is located at the bottom of the cleft between the two domains. Three additional X-ray structures of SDH bound to a sulfate anion, adenosine monophosphate (AMP), and oxalylglycine (OxGly) have been determined.<sup>10</sup> The sulfate-bound structure revealed features of how the  $\alpha$ -keto acid substrate binds to R131 in the active site and showed a modest closure of the cleft between domains I and II. AMP was found to bind in the active site region expected to be occupied by the dinucleotide cofactor NAD. OxGly, an analogue of  $\alpha$ -kg, was observed to bind to two arginines, R18 and R131 in the active site. A semiempirical model was proposed on the basis of these ligand-bound structures with NAD and Sacc modeled in the active site.

We now report a crystal structure of the ternary E-NADH-Sacc complex for the first time, which shows an enzyme form with a closed active site with K77 and H96 properly positioned to serve as acid–base catalysts. Mutant enzymes were characterized via the pH dependence of kinetic

parameters and isotope effects. Data are discussed in terms of the proposed mechanism of SDH.

## MATERIALS AND METHODS

**Chemicals.** Ampicillin, chloramphenicol, Sacc, Lys,  $\alpha$ -kg, AMP, OxGly, polyethylene glycol 3350, Bis-Tris propane, horse liver alcohol dehydrogenase, yeast aldehyde dehydrogenase, and the GenElute plasmid mini preparation kit were obtained from Sigma.  $\beta$ -NADH,  $\beta$ -NAD, Luria-Bertani (LB) broth, LB agar, and imidazole were purchased from U.S. Biochemical Corp. The buffers, Ches, Taps, Hepes, and Mes, were from Research Organics, while Ni-NTA resin was purchased from 5 Prime. Ethanol- $d_6$  (99 atom % D) and  $D_2O$  (99.9 atom % D) were purchased from Cambridge Isotope Laboratories. Ethanol (absolute, anhydrous) was from Pharmaco-Aaper. Polyethylene glycol monomethyl ether (PEG-MME) and sodium malonate were from Hampton Research. Isopropyl  $\beta$ -D-1-thiogalactopyranoside was from Invitrogen. The QuikChange site-directed mutagenesis kit was from Stratagene, which includes PfuTurbo DNA polymerase and the *DpnI* restriction enzyme. (4R)-4-<sup>2</sup>H NADH (NADD) was prepared as described previously.<sup>11</sup> The concentration of NADD was estimated using an  $\epsilon_{340}$  of 6220 M<sup>-1</sup> cm<sup>-1</sup>. All chemicals were obtained commercially, were of the highest grade available, and were used without further purification.

**Site-Directed Mutagenesis.** Template DNA used for site-directed mutagenesis was the plasmid containing the C205S mutation of SDH,<sup>1</sup> to change K77 and H96 to M and Q, respectively. The following forward and reverse primers were used to generate the K77M mutant enzyme: K77<sub>F</sub>, 5'-CATTATAGGTTTGATGGAAATGCCTGAAACCG-3'; K77<sub>R</sub>, 5'-CGGTTTCAGGCATTTCCATCAAACCTATAA-3'. The following primers were used to generate the H96Q mutant enzyme: H96<sub>F</sub>, 5'-CATCCAGTTTGCTCAGTGCTACAAAGACCAAGC-3'; H96<sub>R</sub>, 5'-GCTTGGTCTTTGTAGCACTGAGCAAACCTGGATG-3'. In addition, a double-mutant enzyme was prepared using the K77M forward and reverse primers and the H96Q mutant gene to generate K77M/H96Q. The mutated codon is shown in bold. Polymerase chain reaction followed by mutagenesis was conducted according to

the instructions in the QuikChange site-directed mutagenesis kit as described previously.<sup>7</sup> The XL-1-Blue competent cell strain of *Escherichia coli* was transformed with the plasmids containing mutations. Plasmids were isolated and purified using the GenElute plasmid mini preparation kit (Sigma). Mutations were confirmed by sequencing the entire gene at the Sequencing Core of the Oklahoma Medical Research Foundation (Oklahoma City, OK).

**Expression and Purification.** *E. coli* BL21 (DE3)-RIL cells were transformed with plasmids containing mutant genes, and expression was conducted as reported previously<sup>5</sup> with some modifications. Once the cell density reached an  $A_{600}$  of 0.3–0.4, induction of protein expression was conducted at 37 °C by addition of 0.2 mM IPTG, followed by incubation for 3–4 h. Cells were harvested by centrifugation at 10000g for 10 min and then sonicated in 100 mM Hepes (pH 7.5) containing 300 mM NaCl and 5 mM imidazole. Enzymes were purified by Ni-NTA affinity chromatography, with elution using 300 mM imidazole. The enzymes were >95% pure as judged by sodium dodecyl sulfate–polyacrylamide gel electrophoresis (SDS–PAGE). The enzymes were stored at 4 °C in elution buffer.

**Enzyme Assay.** Initial velocities were measured using a Beckman DU 640 UV–visible spectrophotometer. All assays were performed at 25 °C. Enzyme activity was measured in quartz cuvettes with a path length of 1 cm in the direction of Sacc formation by monitoring the decrease in  $A_{340}$  ( $\epsilon_{340} = 6220 \text{ M}^{-1} \text{ cm}^{-1}$ ) as NADH is oxidized. When NADH had to be maintained at high concentrations, the reaction was monitored at 366 nm ( $\epsilon_{366} = 3110 \text{ M}^{-1} \text{ cm}^{-1}$ ) using a path length of 0.4 cm. Reactions were initiated by addition of enzyme to a reaction mixture with a final volume of 0.5 mL containing 100 mM Hepes (pH 7.0), a saturating level of NADH (0.5 mM), and variable concentrations of  $\alpha$ -kg and Lys.

**pH Studies.** The pH dependence of  $V$ ,  $V/K_{\text{Lys}}$ , and  $V/K_{\alpha\text{-kg}}$  was measured over the pH range of 5–10 at 0.5 mM NADH and either  $\alpha$ -kg or Lys kept at a saturation concentration while the other was varied. Buffers were maintained at 100 mM in the following pH range: pH 5.5–7.0 for Mes, pH 7.0–8.0 for Hepes, pH 8.0–9.0 for Taps, and pH 9.0–10.0 for Ches. None of the buffers had any effect on the activity of any of the mutant enzymes. The pH was recorded before and immediately after the reaction; no significant differences were detected. To be certain that the kinetic mechanism of the enzyme did not change with pH and to obtain estimates of  $K_m$  values for both substrates at the pH extremes, we obtained initial velocity patterns at extreme pH values (5.5 and 10.0) with the  $\alpha$ -kg and Lys concentrations varied, and NADH was maintained at a saturating concentration (0.5 mM).

**Kinetic Isotope Effects.** Isotope effects were measured for K77M and H96Q mutant enzymes in the pH-independent region of their pH–rate profiles (pH 9). Isotope effects on  $V_2$  and  $V_2/K_{\text{Lys}}$  were measured with NADH(D) ( $10K_m$ ) and  $\alpha$ -kg ( $10K_m$ ) maintained at saturating levels and the Lys concentration varied. Solvent deuterium kinetic isotope effects were measured at pH(D) 9, in the pH-independent region of the pH(D)–rate profiles. For rates measured in  $\text{D}_2\text{O}$ , substrates ( $\alpha$ -kg and Lys) and buffers were first dissolved in a small amount of  $\text{D}_2\text{O}$  and then lyophilized to replace exchangeable protons. The lyophilized powders were then redissolved in  $\text{D}_2\text{O}$  to give the desired concentrations, and the pD was adjusted using either DCl or NaOD. NADH was dissolved in  $\text{D}_2\text{O}$  directly. Reactions were initiated via addition of a small amount of each of the mutant enzymes in  $\text{H}_2\text{O}$ ; the

final concentration of  $\text{D}_2\text{O}$  in the reaction mixture was ~98%. Multiple isotope effects were determined by direct comparison of the initial rates in  $\text{H}_2\text{O}$  and  $\text{D}_2\text{O}$  as for solvent deuterium effects, varying the lysine concentration at fixed saturating concentration of NADD and  $\alpha$ -kg.

**Viscosity Effects.** Initial velocities were determined in  $\text{H}_2\text{O}$  at a relative viscosity of 1.24 at pH 8.0 and 25 °C. Assays contained 9% (w/v) glycerol as the viscosogen, which generates the same relative viscosity as 100%  $\text{D}_2\text{O}$  at 25 °C.<sup>12</sup> The effects of viscosity on  $V$  and  $V/K$  [ $^nV$  and  $^n(V/K)$ ] were determined as the ratio of  $V$  and  $V/K$  in the absence and presence of glycerol.

**Data Analysis.** Initial rate data were first analyzed graphically by double-reciprocal plots to determine the quality of the data and the proper rate equation for data fitting. Data were then fit using the appropriate equations<sup>2</sup> using the Marquardt–Levenberg algorithm,<sup>13</sup> supplied with the Enzfitter program from BIOSOFT (Cambridge, U.K.). Kinetic parameters and their corresponding standard errors were estimated using a simple weighing method.

Data from saturation curves for pH–rate profiles and viscosity effects were fit to eq 1. Data obtained from the initial velocity patterns were fit to eq 2. Data for  $V$  and  $V/K$  deuterium isotope effects were fit using eqs 3 and 4. Equal isotope effects on  $V$  and  $V/K$  are assumed in eq 3, while the isotope effects on  $V$  and  $V/K$  are allowed to be independent in eq 4. The SE of a product or dividend was estimated using eq 5.

$$v = \frac{VA}{K_a + A} \quad (1)$$

$$v = \frac{VAB}{K_{ia}K_b + K_aB + K_bA + AB} \quad (2)$$

$$v = \frac{VA}{(K_a + A)(1 + F_i E_v)} \quad (3)$$

$$v = \frac{VA}{K_a(1 + F_i E_{V/K}) + A(1 + F_i E_v)} \quad (4)$$

$$\text{SE } \frac{x}{y} = \frac{x}{y} \left( \frac{\text{SE } x^2}{x^2} + \frac{\text{SE } y^2}{y^2} \right)^{1/2} \quad (5)$$

In eqs 1–4,  $v$  and  $V$  are initial and maximal velocities, respectively,  $A$  and  $B$  are substrate concentrations,  $K_a$  and  $K_b$  are Michaelis constants for substrates  $A$  and  $B$ , respectively, and  $K_{ia}$  is the dissociation constant for dissociation of  $A$  from the EA complex. In eqs 3 and 4,  $F_i$  is the fraction of label in substrate or solvent and  $E_v$ ,  $E_{V/K}$ , and  $E_{V/K}$  are isotope effects minus 1 for the equal isotope effects on  $V$  and  $V/K$  and the independent isotope effects on  $V$  and  $V/K$ , respectively. In eq 5, SE  $x$  and SE  $y$  are computer-generated standard errors of values for kinetic parameters  $x$  and  $y$ , respectively.

Data for pH–rate profiles exhibiting a partial change on the acid side were fit to eq 6.

$$\log y = \log \left[ Y_L + Y_H \left( \frac{H}{K_1} \right) / \left( 1 + \frac{H}{K_1} \right) \right] \quad (6)$$

In eq 6,  $y$  is the observed value of  $V$  or  $V/K$  at any pH,  $H$  is the hydrogen ion concentration,  $K_1$  is the acid dissociation constant of the functional group required in a given protonation state on the enzyme or substrate for optimal binding and/or catalysis,

Table 1. Data Collection and Refinement Statistics

	C205S apoenzyme	Sacc and NADH bound
	Data Collection <sup>a</sup>	
space group	P2 <sub>1</sub> 2 <sub>1</sub> 2 <sub>1</sub>	P4 <sub>3</sub>
unit cell dimensions (Å)	64.95, 75.23, 75.31	68.88, 68.88, 101.85
wavelength (Å)	1.5418	1.5418
temperature (K)	100	100
resolution (Å)	41.71–2.01 (2.12–2.01)	35.2–2.17 (2.29–2.17)
no. of observations	98649	89656
no. of unique reflections	24396	25006
completeness (%)	97.1 (81.8)	99.8 (99.8)
average multiplicity	4.0 (2.6)	3.6 (3.4)
$\langle I/\sigma I \rangle$	15.8 (3.0)	14.5 (3.4)
$R_{\text{merge}}^b$	0.052 (0.295)	0.063 (0.300)
	Refinement	
no. of protein atoms	2921	2884
no. of solvent atoms	152	134
no. of ligand atoms	0	69
average <i>B</i> factor (all atoms)	25.01	24.37
$R_{\text{cryst}}^c$	0.197	0.178
$R_{\text{free}}^d$	0.273	0.228
rmsd <sup>e</sup>		
bond lengths (Å)	0.022	0.022
bond angles (deg)	1.74	1.89
Ramachandran plot (%) <sup>f</sup>		
favored	97.8	97.5
allowed	2.2	2.5
outliers	0.00	0.00
disallowed	0.00	0.00

<sup>a</sup>The data in parentheses refer to the highest-resolution shell. <sup>b</sup> $R_{\text{merge}} = \sum_h \sum_l |I_{hi} - \langle I_h \rangle| / \sum_h \sum_l \langle I_h \rangle$ , where  $I_{hi}$  is the *i*th observation for unique *hkl* *h* and  $\langle I_h \rangle$  is the mean intensity for unique *hkl* *h*. <sup>c</sup> $R_{\text{cryst}} = \sum |F_o| - |F_c| / \sum |F_o|$ , where  $F_o$  and  $F_c$  are the observed and calculated structure factors, respectively. <sup>d</sup> $R_{\text{free}}$  was calculated using the 5% of the randomly selected diffraction data that were excluded from the refinement. <sup>e</sup>Ideal values of the root-mean-square deviation (rmsd) taken from ref 16. <sup>f</sup>Calculated using MolProbity.<sup>22</sup>

and  $Y_L$  and  $Y_H$  are pH-independent constant values of  $y$  at low and high pH, respectively.

**Crystallization.** The purified SDH C205S mutant enzyme was crystallized on the basis of fine screening of the conditions described by Andi et al.<sup>10</sup> for the SDH wild-type apoenzyme. The final reservoir for crystallization of the SDH C205S enzyme contained 100 mM Tris (pH 7.0) and 30% (w/v) PEG-MME 2000 at 4 °C using the hanging drop vapor diffusion method. The hanging drop contained equal volumes of protein [14–18 mg/mL in 0.1 M Hepes (pH 7.0)] and reservoir solution (2  $\mu$ L each). Trays were cooled and set up at 4 °C.

Diffraction quality crystals could not be obtained by soaking Sacc and NADH into the apo-C205S SDH crystals. Likewise, cocrystallization trials with the SDH C205S enzyme with Sacc and NADH using the original apo-SDH conditions did not produce diffraction quality crystals. New cocrystallization conditions were determined on the basis of broad screen crystallization trials conducted using the Mosquito liquid handler from TTP Labtech. A series of optimization screens were developed by varying the concentrations of polyethylene glycol (PEG) 3350 from 10 to 25% (w/v) and malonate from 0 to 0.3 M with 0.1 M Bis-Tris Propane (pH 6.5). Trials were set up in 24-well VDX crystallization plates using a Rigaku Automation Alchemist II liquid handler. The final conditions that yielded diffraction quality crystals of the E-Sacc-NADH complex included 22% PEG 3350, 0.3 M malonate, and 0.1 M Bis-Tris Propane (pH 6.5) at 4 °C.

**X-ray Data Collection.** All data was collected at 100 K, and crystals were cryoprotected by being transferred through increasing concentrations of glycerol to a final concentration of 15%. All crystals were rapidly cryocooled in liquid nitrogen.

X-ray data for the C205S apoenzyme and E-Sacc-NADH complex crystals were collected at 100 K using Cu  $K\alpha$  ( $\lambda = 1.5418$  Å) radiation on a Rigaku RU3HR rotating anode generator and RAXIS IV<sup>++</sup> image plate detector. Diffraction data were integrated using Mosflm and scaled and merged using SCALA, and structure factors were calculated using TRUNCATE as found in the CCP4 program suite.<sup>14</sup> Data collection statistics are listed in Table 1.

**Molecular Replacement.** Initial phasing for both structures was conducted by molecular replacement using PHASER.<sup>15</sup> The native apoenzyme structure [Protein Data Bank (PDB) entry 2Q99] was used as the initial search model for the apo-C205S structure.<sup>9</sup> The resultant C205S structure was used as a search model in molecular replacement to determine the E-Sacc-NADH structure. There is a significant conformational change that occurs upon binding of Sacc and NADH, and as a result, the apoenzyme model had to be edited by being separated into two halves at residues Phe135 and Pro326. Refinement was conducted using REFMAC,<sup>16</sup> with a round of simulated annealing conducted initially in PHENIX<sup>17</sup> to reduce model bias. Model visualization, rebuilding, and the fitting of Sacc and NADH were done using COOT.<sup>18</sup> Water molecules were added toward the end of the refinement using the Add Waters function in COOT and visually inspected after



the initial placement. A glycerol molecule was also found in the ligand-bound structure. Refinement statistics are listed in Table 1.

**Molecular Graphics.** Structural figures were prepared using PyMOL version 1.2b6pre.<sup>19</sup>

## RESULTS

**Cell Growth, Expression, and Purification.** Expression of the K77M/C205S, H96Q/C205S, and K77M/H96Q/C205S mutant enzymes was similar to that of wild-type (WT) SDH. All enzymes eluted from the Ni-NTA column with buffer containing 300 mM imidazole (pH 8). The purity of the proteins was assessed by SDS-PAGE, and all of the mutant proteins were estimated to be >95% pure. The His-tagged mutant enzymes maintained stability and remained active for months when stored at 4 °C in 100 mM Hepes, 300 mM KCl, and 300 mM imidazole (pH 8).

**Structural Studies.** The X-ray structure of the pseudo-WT C205S apoenzyme (PDB entry 3UGK) was determined from crystals grown as described in Materials and Methods.

Diffraction data indicated a space group of  $P2_12_12_1$ , and the highest-resolution shell was 2.01 Å (Table 1). The structure was determined by molecular replacement and initially built from the SDH model (PDB entry 2Q99) published by Berghuis and colleagues.<sup>9</sup> The structure of the C205S apoenzyme is virtually identical to that of the WT enzyme. A superimposition of the two structures gives a root-mean-square deviation of 0.31 Å (data not shown).

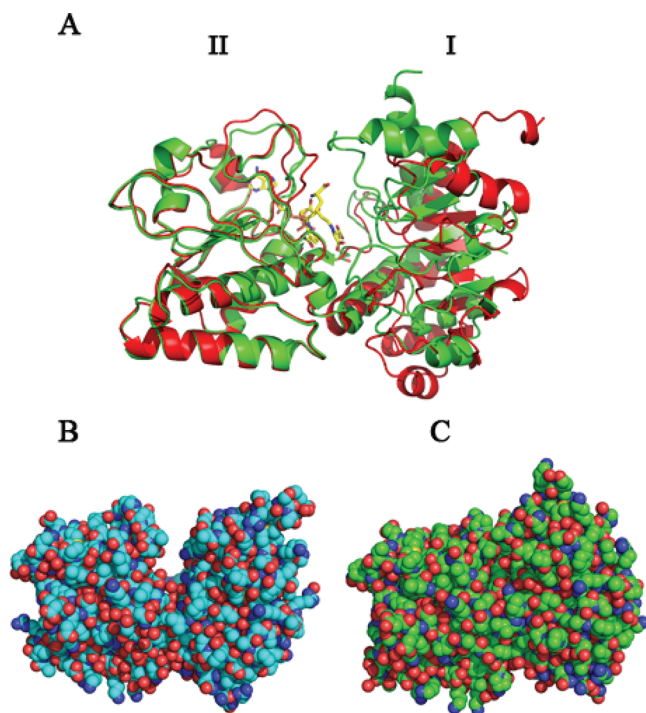


**Figure 1.** Overall structures of the C205S apoenzyme and E-NADH-saccharopine ternary complex. (A) Superimposition of the apoenzyme (red) and ternary complex (green). Note the change in the position of the loop and helix in domain I (right) to close the active site. Stick models of NADH and saccharopine are shown bound to domain II (left). (B) CPK model of the apoenzyme with the active site entrance at the top (same orientation as in panel A). (C) CPK model of the ternary complex structure in the same orientation as shown in panel B.

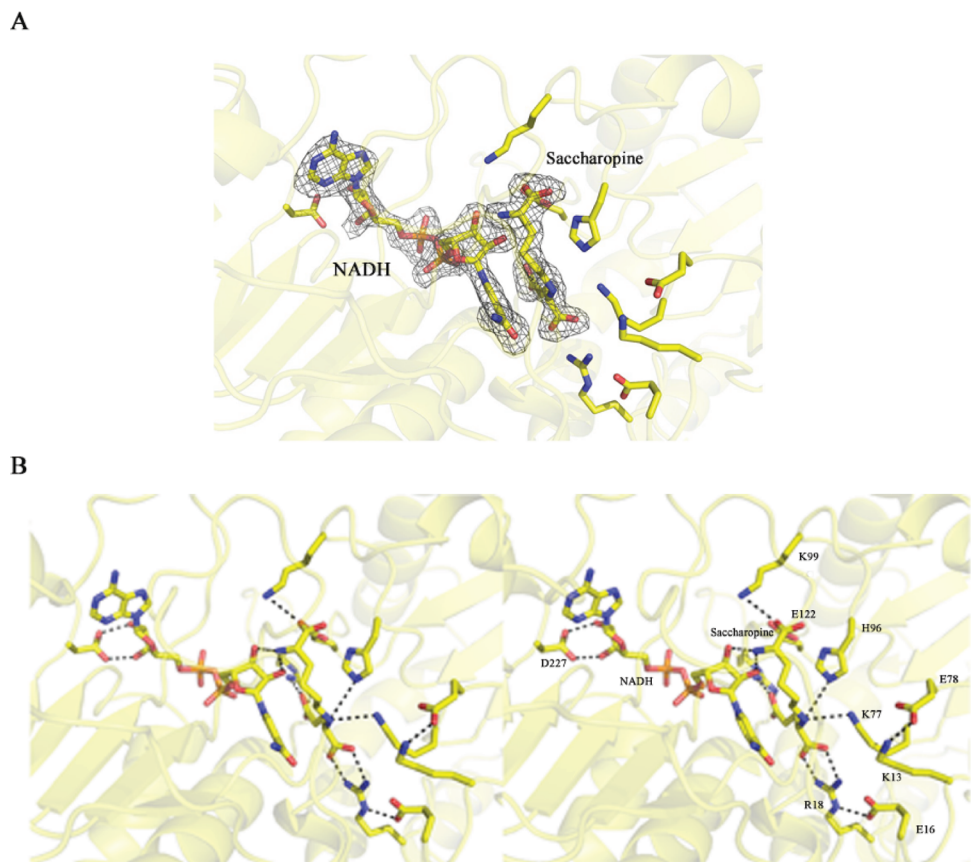
Attempts to crystallize a ternary complex of the WT enzyme were unsuccessful, likely as a result of very weak binding of the cofactor to the enzyme with an oxidized disulfide.<sup>1</sup> A ternary complex structure was obtained by cocrystallization of the C205S enzyme with Sacc and NADH (PDB entry 3UH1). Diffraction data indicated a space group of  $P4_3$ , and the highest-resolution shell was 2.17 Å (Table 1). The structure was determined by molecular replacement using the structure of the C205S apoenzyme as discussed in Materials and Methods. A superimposition of the E-Sacc-NADH ternary complex structure with the C205S apoenzyme structure indicated significant changes that result in a closure of the active site (Figure 1A). In the ternary complex, there is a slight rotation and rigid body movement of almost 9 Å of domain I toward domain II that effectively closes the cleft region as shown in the CPK models in Figure 1B (apo) versus Figure 1C (ternary complex). The net displacement of K99 in the C97–K103 loop region is 8.8 Å in the ternary complex relative to the apoenzyme.

Figure 2A shows an  $F_o - F_c$  difference electron density map of the active site region to illustrate the positions of the bound NADH and Sacc molecules. Figure 2B is a stereoview of the active site with hydrogen bond and ionic interactions shown for protein side chains in contact with the ligands. The distances between enzyme side chain atoms and reactants are listed in Table 2. The Nε atom of K77 and the Nε2 atom of H96 form hydrogen bonds with the Nε atom of Sacc. Other important contacts are made through R18 and E122. Also shown is an ionic interaction between D227 and NADH. There are several hydrogen bond interactions between the cofactor NADH and the substrate saccharopine.

We also attempted to cocrystallize SDH with NADH and lysine using the same screening conditions that were used for the E-Sacc-NADH ternary complex crystals. However, we observed density for only NADH in the determined structure (PDB entry 3UHA), and the enzyme was observed to be in the open conformation (data not shown).

**Initial Velocity Studies.** Initial velocities were measured in the direction of Sacc formation for the K77M, H96Q, and K77M/H96Q mutant enzymes. Replacing K77 with M resulted in a 145-fold decrease in  $V_2/E_t$  and  $>10^4$ - and  $>10^3$ -fold decreases in  $V_2/K_{\alpha\text{-kg}}E_t$  and  $V_2/K_{\text{Lys}}E_t$ , respectively. This results in 28- and 90-fold increases in  $K_{\text{Lys}}$  and  $K_{\alpha\text{-kg}}$ , respectively. Replacing H96 with Q resulted in a 28-fold decrease in  $V_2/E_t$  and  $>10^3$ -fold decreases in  $V_2/K_{\alpha\text{-kg}}E_t$  and  $V_2/K_{\text{Lys}}E_t$ .  $K_{\alpha\text{-kg}}$  and  $K_{\text{Lys}}$  increased 80- and 300-fold, respectively. The K77M/H96Q double mutant gave the largest changes in kinetic parameters, as expected, with 660-,  $>10^6$ -, and  $\sim 10^5$ -fold decreases in  $V_2/E_t$ ,  $V_2/K_{\alpha\text{-kg}}E_t$ , and  $V_2/K_{\text{Lys}}E_t$ , respectively.  $K_{\alpha\text{-kg}}$  and  $K_{\text{Lys}}$  increased  $>10^3$ - and  $10^2$ -fold, respectively. Kinetic parameters are summarized in Table 3 and compared to those obtained for the pseudo-WT, C205S.<sup>1</sup>

**pH Dependence of Kinetic Parameters.** The pH dependence of kinetic parameters provides information about the optimal protonation state of functional groups on the enzyme and/or substrate for binding and/or catalysis. Studies were conducted with K77M and H96Q mutant enzymes in the direction of saccharopine formation, at 25 °C; the rate obtained with the double mutant was too low to allow data to be collected as a function of pH. Both mutant enzymes were active and stable over the pH range of 5–10, and initial rate studies at pH 5.5 and 10 suggest the kinetic mechanism did not change (data not shown). For the K77M mutant enzyme,  $V_2/K_{\text{Lys}}E_t$  is



**Figure 2.** Close-up view of the active site of SDH in the ternary complex with NADH and saccharopine. (A) Monoview of an  $F_0 - F_c$  difference electron density map contoured at  $3\sigma$  with ligand atoms omitted. (B) Stereoview of the active site with NADH and saccharopine bound. Residues within hydrogen bonding distance (shown as a dashed line) of NADH and Sacc are shown. Distances represented by the dashes are listed in Table 2.

**Table 2. Distances between Enzyme Side Chains and Reactants**

side chain—reactant	distance (Å)
R18 NH1—Sacc O1	2.8
R18 NH2—Sacc O2	2.8
R131 NH1—Sacc O3	2.8
R131 NH1—Sacc O4	2.6
K77 Ne—Sacc Ne	3.4
H96 Ne2—Sacc Ne	3.5
K13 Ne—Q78 O $\gamma$	2.6
D227 O1—NADH O2	2.6
D227 O1—NADH O3	2.8
NADH C4—Sacc C8 <sup>a</sup>	3.6

<sup>a</sup>Numbering for Sacc is from C1 of the lysine half to C11, the  $\gamma$ -carboxylate of the glutamate half.

**Table 3. Summary of the Kinetic Parameters**

	C205S	K77M <sup>a</sup>	H96Q <sup>a</sup>	K77M/H96Q <sup>a</sup>
$V_2/E_t$ ( $s^{-1}$ )	106	$0.73 \pm 0.02$	$3.83 \pm 0.03$	$0.16 \pm 0.02$
$V_2/K_{t,kg}E_t$ ( $M^{-1}s^{-1}$ )	$9.7 \times 10^5$	$73 \pm 6$	$435 \pm 116$	$0.50 \pm 0.05$
$V_2/K_{Lys}E_t$ ( $M^{-1}s^{-1}$ )	$1.2 \times 10^5$	$29 \pm 2$	$14 \pm 3$	$1.7 \pm 0.8$
$K_{t,kg}$ (mM)	0.11	$10.0 \pm 0.8$	$9 \pm 2$	$267 \pm 60$
$K_{Lys}$ (mM)	0.89	$25 \pm 2$	$267 \pm 60$	$96 \pm 9$

<sup>a</sup>Mutations prepared in the C205S background.<sup>1</sup>

pH-independent while  $V_2/E_t$  exhibits a partial change on the acid side giving a  $pK_a$  of  $\sim 7.4$ . pH-independent values of  $V_2/E_t$  are  $0.20 \pm 0.03 s^{-1}$  at low pH and  $1.4 \pm 0.1 s^{-1}$  at high pH. The average pH-independent value of  $V_2/K_{Lys}E_t$  is  $0.8 \pm 0.5$ . In the case of H96Q,  $V_2/E_t$  exhibits a decrease at low pH with a slope of  $<1$ , giving an apparent  $pK_a$  of  $\sim 6.7$ , while  $V_2/K_{Lys}E_t$  exhibits a partial change with a  $pK_a$  of  $\sim 9$ , decreasing from a constant value at high pH to a lower constant value at low pH. The pH-independent value of  $V_2/E_t$  is  $4.8 \pm 0.3 s^{-1}$ , while values of  $450 \pm 280$  and  $4.5 \pm 2.9 M^{-1} s^{-1}$  are obtained for  $V_2/K_{Lys}E_t$  at high and low pH, respectively.

**Isotope Effects.** Isotope effects were measured for the K77M mutant enzyme at pH 9, the high-pH-independent region of the pH-rate profiles. Values of 1.8 and 2.0 were obtained for  $^D V_2$  and  $^D(V_2/K_{Lys})$ , and both are greater than the value of 1.3 reported for the pseudo-WT enzyme (C205S). A small normal  $^D_2O V$  is observed, but  $^D_2O(V/K_{Lys})$  is the inverse. Repeating the solvent effect with NADD gave only slight changes. On the other hand, a repeat of the primary deuterium effect in  $D_2O$  decreases the isotope effect on  $V$  from 1.8 to 1.4 but causes no change in the isotope effect on  $V_2/K_{Lys}$ .

For H96Q, the primary deuterium isotope effect is unity within error, whether measured in  $H_2O$  or  $D_2O$ . The solvent deuterium kinetic isotope effect is 2.4, and there is no significant change when it is measured with NADD. Data are summarized in Table 4 and compared to those obtained for the C205S mutant enzyme.<sup>1</sup>

**Viscosity Effects.** To determine whether the SKIEs reflect the increased viscosity in  $D_2O$ , the initial rate was measured in

**Table 4. Summary of the Kinetic Isotope Effects<sup>a</sup>**

	C205S <sup>b</sup>	K77M <sup>c,d</sup>	H96Q <sup>c,e</sup>
<sup>D</sup> V	1.3 ± 0.2	1.81 ± 0.02	1.17 ± 0.40
<sup>D</sup> (V/K <sub>Lys</sub> )	1.3 ± 0.2	2.03 ± 0.04	1.17 ± 0.40
<sup>D</sup> <sub>2</sub> O V	1.5 ± 0.1	1.45 ± 0.01	2.43 ± 0.02
<sup>D</sup> <sub>2</sub> O (V/K <sub>Lys</sub> )	1.5 ± 0.1	0.77 ± 0.05	2.43 ± 0.02
<sup>D</sup> <sub>2</sub> O (V) <sub>D</sub>	1.5 ± 0.1	1.32 ± 0.02	2.24 ± 0.05
<sup>D</sup> <sub>2</sub> O (V/K <sub>Lys</sub> ) <sub>D</sub>	1.5 ± 0.1	0.62 ± 0.07	2.24 ± 0.05
<sup>D</sup> (V) <sub>D<sub>2</sub>O</sub>	ND	1.42 ± 0.01	1.06 ± 0.11
<sup>D</sup> (V/K <sub>Lys</sub> ) <sub>D<sub>2</sub>O</sub>	ND	2.03 ± 0.03	1.06 ± 0.11

<sup>a</sup>Isotope effects were measured at pH 9. <sup>b</sup>From ref 1. <sup>c</sup>Errors are the standard error of the mean. <sup>d</sup>Data for K77M were fit to eq 4. <sup>e</sup>Data for H96Q were fit to eq 3.

the absence and presence of 9% glycerol, which gives a relative viscosity of 1.24, the same as that of 100% D<sub>2</sub>O.<sup>20</sup> There was no effect of viscosity on V or V/K for the H96Q mutant enzyme; a value of 1.02 ± 0.01 was obtained. For K77M, <sup>3</sup>V and <sup>3</sup>(V/K) were 1.18 ± 0.03 and 0.61 ± 0.06, respectively.

## DISCUSSION

**Structures.** Previous structures of WT apo-SDH<sup>9</sup> and substrate analogue-bound structures<sup>10</sup> showed an open or partially closed cleft between domains I and II. The E·NADH·Sacc ternary complex structure described here reveals a closed conformation in which reactants are tightly bound to the enzyme via hydrogen bond and ionic interactions and poised for acid–base catalysis. A slight rotation and a 8.8 Å shift of domain I toward domain II are responsible for closing the active site.

On the basis of the E·NADH·Sacc ternary complex of SDH, there are a number of ionizable residues in the active site as discussed in the introductory section, including R18, R131, K99, K77, K13, E122, E78, E16, and H96. A multiple-sequence alignment of the SDH from *S. cerevisiae*, *Candida albicans*, *Aspergillus fumigatus*, *Cryptococcus neoformans*, *Magnaporthe grisea*, *Yarrowia lipolytica*, and *Schizosaccharomyces pombe* indicated that all of these active site residues are conserved in these fungal species (data not shown), consistent with their importance in the mechanism.

As shown in Figure 2A, K77 and H96 are within hydrogen bonding distance (3.4 and 3.5 Å, respectively) of the secondary amine of saccharopine and could serve as acid–base catalysts in the dehydrogenase reaction. The proposed mechanism suggests that one of the residues accepts a proton from the secondary amine in the hydride transfer step, while the second activates water for hydrolysis of the resulting imine. The lysine and imidazole side chains of K77 and H96 are in proper position to conduct these functions. Data presented in Results are in agreement with this hypothesis and further discussed below.

**Kinetic Parameters.** All three mutant enzymes, K77M, H96Q, and K77M/H96Q, were characterized in the direction of Sacc formation. Initial rates measured as a function of reactant concentration suggested the kinetic mechanism did not change compared to that proposed for the C205S pseudo-WT enzyme, i.e., binding of NADH first, followed by random addition of α-kg or Lys (data not shown).

Mutating K77 to M decreases the positive charge at the site, while changing H96 to Q likely does not change the overall charge, assuming the imidazole side chain is neutral at neutral pH. Mutation of K77 gives a 145-fold decrease in V/E<sub>v</sub> the

largest thus far observed for any site-directed mutation in SDH.<sup>7,8</sup> The 2 order of magnitude decrease in the turnover number and 3–4 order of magnitude decreases in the second-order rate constants are consistent with the K77 side chain playing a direct role as an acid–base catalyst in the SDH reaction. Substitution of a glutamine for H96 leads to a 28-fold decrease in the turnover number of SDH and >3 order of magnitude decreases in second-order rate constants. Although the decreases are not as great as those observed for the K77M mutant enzyme, the data are suggestive of a catalytic role for H96. In agreement, the double-mutant enzyme, K77M/H96Q, gives a nearly 3 order of magnitude decrease in V<sub>2</sub>/E<sub>t</sub> and 5–6 order of magnitude decreases in the second-order rate constants. These data, together with the position of the two residues in the site, are consistent with their role as acid–base catalysts in the reaction.

**Isotope Effects.** Primary and solvent isotope effects are sensitive tools for investigating the slow step or rate-determining steps in the reaction. The primary deuterium kinetic isotope effect (PKIE) reflects the hydride transfer step (see Scheme 1).<sup>6</sup> A solvent kinetic isotope effect (SKIE) is observed when protons are in flight in transition states that contribute to rate limitation. In the WT and C205S enzymes, the SKIE was derived from protons in flight in the hydride transfer and imine hydrolysis steps, corroborated by a concave downward proton inventory.<sup>6</sup>

The maximal rate for the C205S mutant enzyme is slightly pH-dependent, decreasing from a constant value at high pH to another constant value at low pH. The isotope effects for the C205S enzyme reported in Table 4 were measured at pH 9.<sup>1</sup> The effects obtained at pH 5.6 equal ~2, similar to the value obtained for the K77M mutant at pH 9. The data suggest hydride transfer is slower for the K77M mutant enzyme. The slightly smaller isotope effect on V suggests release of NAD or isomerization of the E·NADH complex contributed to rate limitation. The SKIE on V is similar to that obtained for C205S, but the effect on V/K<sub>Lys</sub> is unexpectedly inverse and will be discussed further below. A repeat of the PKIE in D<sub>2</sub>O gives a value for <sup>D</sup>(V/K<sub>Lys</sub>) equal to that obtained in H<sub>2</sub>O, suggesting that the hydride transfer step is rate-determining at pH 9, and the observed solvent deuterium isotope effect reflects changes that occur or have occurred once the transition state for hydride transfer is attained. The PKIE on V in D<sub>2</sub>O decreases slightly, consistent with a step in addition to hydride transfer contributing to rate limitation; the data are consistent with the suggestion that release of NAD or isomerization of the E·NADH complex contributed to rate limitation. A repeat of the SKIE with NADD fixed gives values that are either identical to or decreased slightly compared to the value in H<sub>2</sub>O. Taken together, the data indicate hydride transfer as the step that is largely rate-determining at limiting Lys (V/K<sub>Lys</sub>) and is a major contributor to rate limitation at saturating reactant concentrations. Thus, as suggested on the basis of structural studies and pH–rate profiles (see below), K77 is, in all likelihood, the base that donates a proton to the secondary amine of Sacc in the hydride transfer step as the imine is reduced.

Inverse SKIEs are expected for ionization of a thiol, hydrolysis of metal-bound H<sub>2</sub>O, a medium effect,<sup>20</sup> or an effect derived from the increase in viscosity generated by D<sub>2</sub>O. Although there is a thiol in the vicinity of the dinucleotide-binding site, it is unlikely this ionization contributes to the chemistry in the site. If anything, it would be expected to decrease the affinity of enzyme for NADH, and this is not



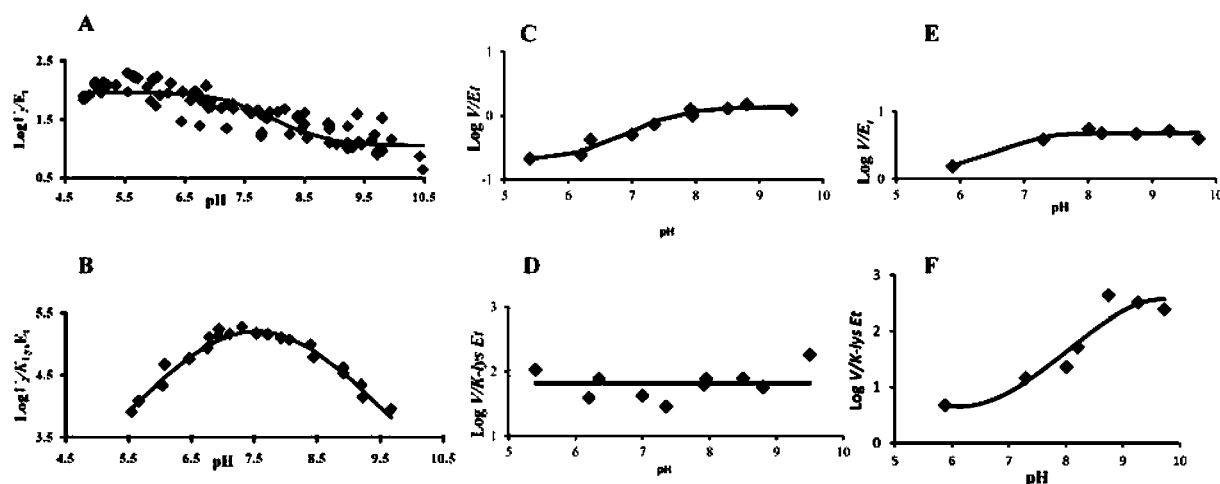


**Figure 3.** pH dependence of kinetic parameters for WT SDH (C205S), K77M/C205S, and H96Q/C205S in the direction of saccharopine formation. Data for the pseudo-WT SDH (C205S) (A and B) are from ref 1 and are reproduced with permission; panels C and D show data for K77M/C205S and panels E and F data for H96Q/C205S. Units for  $V/E_i$  and  $V/K_{\text{lys}} E_i$  are  $\text{s}^{-1}$  and  $\text{M}^{-1} \text{s}^{-1}$ , respectively. Points are the experimentally determined values. The curves are theoretical and based on fits to eq 6 for panels C, E, and F.

observed. There is no metal ion involved in the SDH reaction. It is thus possible that either an effect of the medium or an effect of viscosity is responsible for the observed inverse SKIE and may reflect the conformational change to close the site to form the productive Michaelis complex upon binding of Lys. The viscosity effect is identical to the measured SKIE, consistent with a preference for the closed conformation because of the higher viscosity of  $\text{D}_2\text{O}$ .

The solvent isotope effects, listed in Table 4, are nearly identical to the viscosity effects obtained for K77M. Data strongly suggest the inverse isotope effect on  $V/K$  is a consequence of the change in solvent viscosity in  $\text{D}_2\text{O}$ ; i.e., the solvent deuterium isotope effect on  $V/K$  is 1.0, while a slight normal isotope effect of  $\sim 1.23 \pm 0.02$  ( $1.45/1.18$ ) is observed on  $V$ . Effects near unity suggest proton transfer steps do not contribute or contribute to a very small extent to the rate limitation in the reaction with Lys. The reason for the increased rate in the presence of a viscosogen is not known at this point but likely results from stabilization of an enzyme conformation along the reaction pathway as suggested above. At saturating reactant concentrations, there is a slight contribution from diffusion (viscosity effect) and there is at least one proton in flight in a step that contributes to rate limitation. As suggested above, the step reflects either release of NAD or isomerization of the E-NADH complex, and the presence of a contribution from diffusion suggests that it is likely release of NAD.

Observation of an inverse viscosity effect is not unique to SDH. Similar observations have been made for the *Ascaris suum* NAD malic enzyme<sup>20</sup> and the homoisocitrate dehydrogenase from *S. cerevisiae*<sup>21</sup> using 9% glycerol as the viscosogen. Inverse solvent deuterium isotope effects and viscosity effects of  $\sim 0.8$  and  $\sim 0.5$  were estimated on  $V$  and  $V/K_{\text{malate}}$ , respectively, for the malic enzyme. These results, with a larger inverse effect on  $V/K$  than  $V$ , are qualitatively identical to our results presented here. Data were interpreted in terms of stabilizing the closed form of the enzyme at higher viscosities. The increase in rate is thus a result of an increase in the concentration of the productive Michaelis complex. Isocitrate, a slow substrate for homoisocitrate dehydrogenase, also gave similar inverse solvent isotope and viscosity effects of 0.8 and 0.6 on  $V$  and  $V/K_{\text{iso}}$ ,

respectively. Data were again interpreted in terms of stabilizing an enzyme form along the reaction pathway.

Isotope effects measured for H96Q are very straightforward and easy to interpret. A primary deuterium effect of  $\sim 1$  indicates the hydride transfer step does not contribute to rate limitation. The SKIE is  $\sim 2.3$  on  $V$  and  $V/K_{\text{lys}}$ , significantly greater than the value obtained for C205S. Data are consistent with the proposed role of H96 in formation of the imine prior to its reduction in the hydride transfer step.

**pH Dependence of Kinetic Parameters.** To further probe the role of K77 and H96, the pH dependence of kinetic parameters was measured. These studies allow a determination of the optimal protonation state of the functional groups on the enzyme and/or substrate involved in either binding or catalysis. On the basis of the above discussion, the proposed general base in the direction of Sacc formation is K77, which must accept a proton from the  $\epsilon$ -amine of Lys as it attacks the  $\alpha$ -carbonyl of  $\alpha$ -kg to form the imine. Histidine 96 is proposed to serve a role as a general acid in the reaction, first protonating the carbonyl oxygen to form the protonated carbinolamine, accepting a proton from the protonated carbinolamine to generate the neutral carbinolamine, and eventually protonating the leaving hydroxide to give water (III in Scheme 1).

Data for the C205S mutant enzyme<sup>1</sup> are shown in Figure 3 as a reference for interpreting the pH–rate profiles for K77M and H96Q.  $V_2$  decreases from a constant value at low pH to a lower constant value at high pH. The  $\text{pK}_a$  estimated for the change is 7.5, and the ratio of the constant values is  $\sim 9$ . The pH dependence was attributed to a conformational change in enzyme, with the low-pH conformation being the more active of the two. (This aspect will be discussed further below.) The  $V/K$  for Lys exhibits a bell-shaped pH–rate profile with  $\text{pK}_a$  values of 7 and 8.1 attributed to the general base and general acid, respectively, in the SDH reaction.

Data for the K77M mutant enzyme differ considerably. The  $V_2$  pH–rate profile exhibits a partial change but requires that the group be unprotonated, opposite the situation for C205S. It is clear that the presence of the K77 side chain influences the  $\text{pK}_a$  and perhaps the group responsible for pH-dependent conformational change. On the basis of the isotope effects presented in Results and discussed above, the hydride transfer



step is slow for the K77M mutant enzyme, and we propose that K77 donates a proton as the imine is reduced to the secondary amine in Sacc. The loss of the side chain of K77 results in a significant decrease in the rate at low pH, which increases with an increase in pH, giving a  $pK_a$  of  $\sim 7.5$ . The data obtained in these studies suggest an interpretation that is an alternative to a pH-dependent conformational change. Although chemistry contributes to rate limitation for the pseudo-WT enzyme, the conformational changes required to close the site prior to catalysis and open it prior to product release also make significant contributions.<sup>5,8</sup> The pH dependence observed in the  $V_2$  pH-rate profile may reflect two pathways that differ depending on the protonation state of the  $\epsilon$ -amino groups of the Lys substrate and the side chain of K77. For the C205S mutant enzyme, the optimal protonation state exists when the substrate  $\epsilon$ -amine is protonated and the side chain of K77 is unprotonated. The proximity of the side chain of Lys and K77 results in a decrease in the  $pK_a$  of both  $\epsilon$ -amino groups, facilitating the transfer of a proton from one to the other. As the pH increases, the proton shared between the two side chains is lost; the global  $pK_a$  is  $\sim 7.5$  for the Lys-K77 pair on the basis of the observed  $pK_a$  values. Once the residue is unprotonated, the rate decreases by 9-fold, likely as a result of a change in the orientation of the Lys side chain. In the K77M mutant enzyme, the protonation state of the substrate Lys  $\epsilon$ -amine may also contribute to rate limitation at saturating reactant levels. Once bound, the Lys  $\epsilon$ -amine must be unprotonated to act as a nucleophile as it attacks the  $\alpha$ -carbonyl of  $\alpha$ -kg to form the imine. Other active site side chains, e.g., E78, E16, and K13, must abstract the Lys  $\epsilon$ -amine proton, perhaps via the intermediacy of a water molecule. As the pH increases, the  $\epsilon$ -amine of Lys becomes unprotonated (the  $pK_a$  is around 7.5 for the bound substrate) and can serve as a nucleophile, and the rate increases by  $\sim 10$ -fold.

The dominant forms of the enzyme and substrate present when  $V/K_{Lys}$  is measured are the E-NADH- $\alpha$ -kg complex and free Lys.  $V/K_{Lys}$  is pH-independent, while a bell-shaped pH-rate profile was obtained for C205S with  $pK_a$  values of  $\sim 7$  and  $\sim 8$ . Because free Lys is dominant, the observed  $pK_a$  values are on enzyme; the  $pK_a$  values of the  $\alpha$ - and  $\epsilon$ -amino groups of Lys are 9.5 and 10.5, respectively. One of the  $pK_a$  values likely reflects the K77 side chain, and intrinsic values are observed.<sup>a</sup> It is likely the group with a  $pK$  of  $\sim 7$  that reflects the K77 side chain, consistent with the discussion of the  $pK_a$  of 7.5 in the  $V_2/E_t$  pH-rate profile given above. The  $pK_a$  of the H96 side chain is thus  $\sim 8$  and in the absence of the K77 side chain is perturbed to a pH higher than 9.5, perhaps resulting from the influence of E78, which is in the vicinity and no longer neutralized by K77. The absence of the  $pK_a$  value of  $\sim 7$  is consistent with its attribution to K77.

In the case of the H96Q mutant enzyme, interpretation will begin with the  $V/K_{Lys}$  pH-rate profile. Note that the profile exhibits a partial change, decreasing from a constant value at pH  $> 9$  to a lower constant value at pH  $< 6$ ; the ratio of the constant values is  $\sim 100$ . The observed  $pK_a$  of  $\sim 9$  reflects the side chain of K77, while the  $pK_a$  observed at high pH in C205S is absent, consistent with the assignment of H96 as this group. The loss of the H96 side chain resulted in an increase in the  $pK_a$  of K77 from  $\sim 7.5$  to 9, suggesting an influence of the imidazole side chain on the affinity of the K77 side chain for protons. The H96 side chain must be protonated for optimal reaction in the direction of Sacc formation, and the proximity of the positive charge on the imidazole will certainly result in a

decrease in the  $pK_a$  of the  $\epsilon$ -amino groups of K77. The finite rate obtained at low pH suggests K77 is important for catalysis but is not absolutely essential. This is in agreement with the data obtained for the  $V_2/E_t$  pH-rate profiles for C205S, K77M, and H96Q (see below).

The  $V_2/E_t$  pH-rate profile of H96 is similar to that of K77M at face value. However, because the K77 side chain is absent, the  $pK_a$  reflected is that of the bound substrate, Lys. Thus, the bound Lys has a  $pK_a$  of  $\sim 7$ . As the pH increases and the  $\epsilon$ -amino of bound Lys becomes neutral, the rate increases because the amine can now act as a nucleophile in the attack of the  $\alpha$ -carbonyl of  $\alpha$ -kg to form the imine.

**Conclusions.** A structure of a ternary complex of the C205S pseudo-WT enzyme, NADH, and Sacc provided a closed form of the enzyme and a more accurate description of the interactions between enzyme side chains and reactant functional groups compared to the semiempirical model published previously.<sup>10</sup> Importantly, the distance between C4 of the nicotinamide ring and C8 of Sacc is 3.6 Å as shown in Figure 2, a reasonable hydride transfer distance, compared to a distance of  $> 4.5$  Å estimated from the semiempirical model,<sup>10</sup> which was constructed from open forms of the enzyme. The side chains of H96 and K77 now appear properly positioned to act as acid-base catalysts.

Mutation of K77 to M results in 145-fold decrease in  $V/E_t$  and a  $> 3$  order of magnitude increase in the second-order rate constants. Together with the large primary deuterium isotope effect (2.0) and small solvent deuterium isotope effect (1.45), data suggest rate-limiting hydride transfer, consistent with the proposed role of K77 as a general acid in protonating the imine nitrogen concomitant with hydride transfer. In agreement with this proposal,  $V_2/K_{Lys}E_t$  is pH-independent. The H96Q mutation results in an  $\sim 28$ -fold decrease in  $V_2/E_t$  and  $> 10^5$ -fold decreases in the second-order rate constant. A primary deuterium isotope effect near unity and a large solvent deuterium isotope effect (2.4) are consistent with the proposed role of H96 in protonating the leaving hydroxyl as the imine is formed. Elimination of H96 results in a pH-rate profile for  $V_2/K_{Lys}E_t$  that exhibits the  $pK_a$  for K77, which must be unprotonated to accept a proton from the  $\epsilon$ -amine of the substrate Lys so that it can act as a nucleophile. The proposed roles of H96 and K77 are corroborated by the nearly 700-fold decrease in  $V_2/E_t$  and  $> 10^5$ -fold decreases in the second-order rate constants.

## AUTHOR INFORMATION

### Corresponding Author

\*P.F.C.: e-mail, pcook@ou.edu; telephone, (405) 325-4581; fax, (405) 325-6111. A.H.W.: e-mail, awest@ou.edu; telephone, (405) 325-1529; fax, (405) 325-6111.

### Funding

This work was supported by a grant (GM 071417) from the National Institutes of Health and the Grayce B. Kerr Endowment to the University of Oklahoma to support the research of P.F.C.

### Notes

The authors declare no competing financial interest.

## ABBREVIATIONS

AAA,  $\alpha$ -aminoacidate pathway; E, enzyme; SDH, saccharopine dehydrogenase;  $\alpha$ -kg,  $\alpha$ -ketoglutarate; Sacc, L-saccharopine; Lys, L-lysine; NAD,  $\beta$ -nicotinamide adenine dinucleotide (the

positive charge has been omitted for convenience); NADH, reduced  $\beta$ -nicotinamide adenine dinucleotide; NADD, reduced  $\beta$ -nicotinamide adenine dinucleotide with deuterium in the 4R position; OxGly, oxalylglycine; WT, wild type; Mes, 2-(*N*-morpholino)ethanesulfonic acid; Taps, 3-[*N*-tris-(hydroxymethyl)methylamino]propanesulfonic acid; Hepes, *N*-(2-hydroxyethyl)piperazine-*N'*-2-ethanesulfonic acid; Ches, 2-(*N*-cyclohexylamino)ethanesulfonic acid; PEG-MME, polyethylene glycol monomethyl ester; PKIE, primary kinetic isotope effect; SKIE, solvent kinetic isotope effect; MKIE, multiple kinetic isotope effect.

## ■ ADDITIONAL NOTE

<sup>a</sup>A partial change was observed in the  $V_2/E_t$  pH-rate profile of C205S, which was proposed to reflect a pH-dependent conformational change.<sup>1</sup>  $pK_a$  values for the catalytic groups are not observed, suggesting optimal binding of only the correctly protonated forms of the reactants and enzyme. In this case, intrinsic  $pK_a$  values are observed.<sup>2</sup>

## ■ REFERENCES

- (1) Bobyk, K. D., Kim, S. G., Kumar, V. P., Kim, S. K., West, A. H., and Cook, P. F. (2011) The oxidation state of active site thiols determines activity of saccharopine dehydrogenase at low pH. *Arch. Biochem. Biophys.* 513, 71–80.
- (2) Cook, P. F., and Cleland, W. W. (2007) *Enzyme kinetics and mechanism*, Taylor & Francis Group, LLC, New York.
- (3) Xu, H., Andi, B., Qian, J., West, A. H., and Cook, P. F. (2006) The  $\alpha$ -aminoadipate pathway for lysine biosynthesis in fungi. *Cell Biochem. Biophys.* 46, 43–64.
- (4) Zabriskie, T. M., and Jackson, M. D. (2000) Lysine biosynthesis and metabolism in fungi. *Nat. Prod. Rep.* 17, 85–97.
- (5) Xu, H., West, A. H., and Cook, P. F. (2006) Overall Kinetic Mechanism of Saccharopine Dehydrogenase from *Saccharomyces cerevisiae*. *Biochemistry* 45, 12156–12166.
- (6) Xu, H., Alguindigue, S. S., West, A. H., and Cook, P. F. (2007) A proposed proton shuttle mechanism for saccharopine dehydrogenase from *Saccharomyces cerevisiae*. *Biochemistry* 46, 871–882.
- (7) Ekanayake, D. K., Andi, B., Bobyk, K. D., West, A. H., and Cook, P. F. (2010) Glutamates 78 and 122 in the active site of saccharopine dehydrogenase contribute to reactant binding and modulate the basicity of the acid-base catalysts. *J. Biol. Chem.* 285, 20756–20768.
- (8) Ekanayake, D. K., West, A. H., and Cook, P. F. (2011) Contribution of K99 and D319 to substrate binding and catalysis in the saccharopine dehydrogenase reaction. *Arch. Biochem. Biophys.* 514, 8–15.
- (9) Burk, D. L., Hwang, J., Kwok, E., Marrone, L., Goodfellow, V., Dmitrienko, G. I., and Berghuis, A. M. (2007) Structural studies of the final enzyme in the  $\alpha$ -aminoadipate pathway: Saccharopine dehydrogenase from *Saccharomyces cerevisiae*. *J. Mol. Biol.* 373, 745–754.
- (10) Andi, B., Xu, H., Cook, P. F., and West, A. H. (2007) Crystal Structures of Ligand-Bound Saccharopine Dehydrogenase from *Saccharomyces cerevisiae*. *Biochemistry* 46, 12512–12521.
- (11) Viola, R. E., Cook, P. F., and Cleland, W. W. (1979) Stereoselective preparation of deuterated reduced nicotinamide adenine nucleotides and substrates by enzymatic synthesis. *Anal. Biochem.* 96, 334–340.
- (12) Cook, P. F. (1991) in *Enzyme mechanism from isotope effects*, CRC Press, Boca Raton, FL.
- (13) Marquardt, D. W. (1963) An algorithm for least square estimation of nonlinear parameters. *J. Soc. Ind. Appl. Math.* 11, 431–441.
- (14) Winn, M., Ballard, C. C., Cowtan, K. D., Dodson, E. J., Emsley, P., Evans, P. R., Keegan, R. M., Krissinel, E. B., Leslie, A. G. W., McCoy, A., McNicholas, S. J., Murshudov, G. N., Pannu, N. S., Potterton, E. A., Powell, H. R., Read, R. J., Vagin, A., and Wilson, K. S. (2011) Overview of the CCP4 suite and current developments. *Acta Crystallogr. D* 67, 235–242.
- (15) McCoy, A. J., Grosse-Kunstleve, R. W., Adams, P. D., Winn, M. D., Storoni, L. C., and Read, R. J. (2007) Phaser crystallographic software. *J. Appl. Crystallogr.* 40, 658–674.
- (16) Murshudov, G. N., Skubak, P., Lebedev, A. A., Pannu, N. S., Steiner, R. A., Nicholls, R. A., Winn, M. D., Long, F., and Vagin, A. A. (2011) REFMACS for the refinement of macromolecular crystal structures. *Acta Crystallogr. D* 67, 355–367.
- (17) Adams, P. D., Afonine, P. V., Bunkoczi, G., Chen, V. B., Davis, I. W., Echols, N., Headd, J. J., Hung, L.-W., Kapral, G. J., Grosse-Kunstleve, R. W., McCoy, A. J., Moriarty, N. W., Oeffner, R., Read, R. J., Richardson, D. C., Richardson, J. S., Terwilliger, T. C., and Zwart, P. H. (2010) PHENIX: A comprehensive Python-based system for macromolecular structure solution. *Acta Crystallogr. D* 66, 213–221.
- (18) Emsley, P., and Cowtan, K. (2004) Coot: Model-building tools for molecular graphics. *Acta Crystallogr. D* 60, 2126–2132.
- (19) Delano, W. L. (2004) *The PyMOL molecular graphics system*, DeLano Scientific, San Carlos, CA.
- (20) Karsten, W. E., Lai, C.-J., and Cook, P. F. (1995) Inverse solvent isotope effects in the NAD-malic enzyme reaction are the result of the viscosity difference between D<sub>2</sub>O and H<sub>2</sub>O: Implications for solvent isotope effect studies. *J. Am. Chem. Soc.* 117, 914–918.
- (21) Lin, Y., Volkman, J., Nicholas, K. M., Yamamoto, T., Eguchi, T., Nimmo, S. L., West, A. H., and Cook, P. F. (2008) Chemical Mechanism of Homoisocitrate Dehydrogenase from *Saccharomyces cerevisiae*. *Biochemistry* 47, 4169–4180.
- (22) Chen, V. B., Arendall, W. B. III, Headd, J. J., Keedy, D. A., Immormino, R. M., Kapral, G. J., Murry, L. W., Richardson, J. S., and Richardson, D. C. (2010) MolProbity: All-atom structure validation for macromolecular crystallography. *Acta Crystallogr. D* 66, 12–21.